European Journal of Medicinal Chemistry 47 (2012) 399–411

Contents lists available at SciVerse ScienceDirect

European Journal of Medicinal Chemistry

journal homepage: http://www.elsevier.com/locate/ejmech

Original article

Novel palladium(II) and platinum(II) complexes with 1H-benzimidazol-2-ylmethyl-N-(4-bromo-phenyl)-amine: Structural studies and anticancer activity

Nour T. Abdel Ghani, Ahmed M. Mansour*

Chemistry Department, Faculty of Science, Cairo University, Gamaa Street, Giza 12613, Egypt

ARTICLE INFO

Article history:
Received 23 February 2011
Received in revised form
30 October 2011
Accepted 2 November 2011
Available online 15 November 2011

Keywords:
Biological activity
Benzimidazole
DFT
NBO
LANL2DZ

ABSTRACT

$[MLCl_2]$ (L = (1H-benzimidazol-2-ylmethyl)-N-(4-bromo-phenyl)-amine; M = Pd & Pt) and $[PdL(OH_2)_2]\cdot 2X\cdot zH_2O$ (X = Br, I, z = 2; X = SCN, z = 1; X = NO_3, z = 0) complexes have been synthesized as potential anticancer compounds and their structures were elucidated using elemental analysis, spectral, thermal analysis and X-ray powder diffraction. The benzimidazole (L) crystallizes in the space group $P2_1/c$ with a = 8.6660(3) Å, b = 16.6739(7) Å, c = 9.8611(4) Å and β = 113.505(3) ° and forms an infinite chain structure with a trans-zigzag type along the crystallographic axis "a", through the intermolecular H—bond. FT-IR and ^{1}H NMR studies revealed that the ligand L is coordinated to the metal ion *via* the pyridine-type nitrogen (N_{py}) of the benzimidazole ring and secondary amino group (NH_{sec}). Quantum mechanical calculations of energies, geometries, vibrational wavenumbers, and ^{1}H NMR of the benzimidazole L and its complexes were carried out by DFT/B3LYP method combined with 6–31G(d) and LANL2DZ basis sets. Natural bond orbital (NBO) analysis and frontier molecular orbitals (FMO) were performed at B3LYP/LANL2DZ level of theory. The benzimidazole L, in comparison to its metal complexes was screened for its antibacterial activity. The complexes showed cyctotoxic effects against *human breast cancer* (MCF7), *hepatocarcinoma* ($HepG_2$) and *colon carcinoma* cells (HCT). The platinum complex **(6)** exhibited a moderate antitumor activity against MCF7 with IC_{50} = 10.2 μM comparing to that reported for cis-platin 9.91 μM.

1. Introduction

Despite the widespread use of cis-platin as anticancer drug, there is still scope for improvement, with respect to reduced toxicity [1], increased clinical effectiveness, broader spectrum of action, elimination of side effects (e.g., nausea, hearing loss, vomiting, etc.), increased solubility, and the ability to use them in combination with other drugs. Many cis-platin analogues also inhibit tumor growth, and these compounds have at least one N—H group [2] (one of the reasons for choosing the benzimidazole ligand), which is responsible for important hydrogen-bond donor properties, either in the approach of the biological target or the final structure. In this fertile field, three main approaches to design new drugs are currently observed: **(i)** Direct cis-platin analogues or modifications **(ii)** Use of metals other than platinum and **(iii)** Combination of known, active organic drugs with metal compounds [3]. Among the non-platinum compounds with potential for the clinical treatment of human malignancies, palladium derivatives have received considerable interest, because of the structural analogy between the Pt(II) and Pd(II) complexes. The design of Pd(II) compounds with anticancer activity represents an exciting task, since Pd(II) compounds exchange ligands 105 times faster than analogous Pt(II) compounds [4]. Due to this rapid exchange, Pd(II) derivatives do not maintain their structural integrity long enough to reach the pharmacological target. To overcome their high lability, chelating ligands have been used to afford high thermodynamic stabile and kinetically inert Pd(II) complexes [4]. Recently, interests were carried out in the developing of cis-platin analogues with heterocyclic amine ligands [5] e.g. benzothiazole, and benzimidazole.

The benzimidazole scaffold is a useful structural motif for displaying chemical functionality in biologically active molecules. Some of its derivatives have potent biological activities as antitumor, anti-HIV, and antimicrobial agents [6]. At the same time, owing to the coordination ability of azoles, the chelating ligands incorporating benzimidazole groups have been extensively studied

* Corresponding author. Tel.: +20 2 01222211253; fax: +20 2 35728843-3572556.
E-mail address: inorganic_am@yahoo.com (A.M. Mansour).

0223-5234/$ – see front matter © 2011 Elsevier Masson SAS. All rights reserved.
doi:10.1016/j.ejmech.2011.11.008

in the context of modeling biological systems in recent years [7]. Our aim was to take into account all the previously mentioned properties of anticancer drugs and synthesize new Pt(II) and Pd(II) complexes of new N,N donor benzimidazole derivatived cis-platin analogues that could prove to be potent antitumor agents. The structures of ligand (Fig. 1) and its complexes were elucidated by elemental analysis, FT-IR, ^{1}H NMR, MS, UV/vis., thermal and X-ray diffraction. Theoretical calculations using *density functional theory* (DFT) were done in order to correlate between the theoretical and experimental results. Natural bond orbital (NBO) analysis was performed to provide details about the type of hybridization and the nature of bonding in the studied complexes.

2. Experimental

2.1. Synthesis and characterization of ligand (L) and its complexes

All chemicals used in the preparation and investigation of the present study were of reagent grade (Sigma). The benzimidazole L was prepared by condensation of equimolar quantities of 2-chloromethylbenzimidazole [8] with 4-bromoaniline in presence of sodium iodide for about 18 h. Then, the reaction mixture was neutralized and the separated solid was re-crystallized from ethanol.

The solid Pd(II) and Pt(II) complexes of the benzimidazole compound (L) (X = Cl, Br, I, SCN and NO_3) **(1-6)**, were synthesized as demonstrated in Scheme 1. The results of elemental analyses are in a good agreement with those calculated for the suggested formula and the melting point is sharp indicating the purity of the prepared benzimidazole ligand. The molar conductance values of Pd–L **(1)** and Pt–L **(6)** (X = Cl) complexes in DMF indicated the non-electrolytic nature of these complexes, while the higher conductance values of the other complexes suggested their ionic nature.

2.1.1. Data for **L** ($C_{14}H_{12}Br\ N_3$)

Color: Golden yellow. Yield: 85%. MS: m/z = 302 (M^+, calcd. 302), 218, 171, 132, 155, 118, 93, 91 and 77. Anal. Calcd. %C, 55.65; %H, 4.00; %Br, 26.44; %N, 13.91. Found: %C, 55.58; %H, 3.98; %Br, 26.40; %N, 13.87. FT-IR: 3445 (ν(NH)$_{sec}$), 3052 (ν CH^{ass}/Ar), 2829 (ν CH$_2^{ss}$), 1590 (ν C=C^{ss}), and 1308 cm^{-1} ν(C–N)$_{sec}$. ^{1}H NMR (DMSO): δ 12.27 (1H, s, benzimidazolic NH); δ 6.60 (1H, t, H^{13}), δ 6.63 (1H, d, H^{15}), δ 7.19 (1H, t, H^{16}), δ 7.22 (1H, d, H^{18}); δ 7.12, 7.14, 7.48, and 7.50 (4H, m, benzimidazole ring (Bz) (H$^{2,5-7}$)), δ 6.50 (1H, t, NH$_{sec}$), and δ 4.47 (2H, d, CH$_2$). UV/vis. (Ethanol): 206, 225, 249, 273 and 280 nm, and (DMF): 263, 274, and 281 nm.

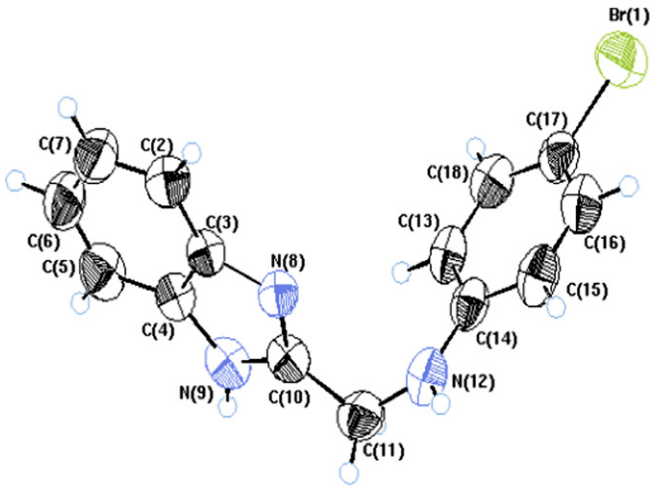

Fig. 1. ORTEP plot of benzimidazole L.

2.1.2. Data for **Pd–L (X = Cl) (1)** ($C_{14}H_{12}BrCl_2N_3Pd$)

Color: Yellow. Yield: 80%. MS: m/z = 478 (M^+, calcd. 478), 328, 301, 258, 241, 223, 220, 192, 171, 131, 118 and 91. Anal. Calcd. %C, 35.07; %H, 2.52; %N, 8.76; %Pd, 22.19. Found: %C, 35.29; %H, 2.79; %N, 8.71; %Pd, 21.99. FT-IR: 3415 (ν(NH)$_{sec}$), 1625 (ν(C=N)), 1447 (ν(NH$_b$)$_{sec}$), 1319 (ν(C–N)$_{Bz}$), and 1281 (ν(C–N)$_{sec}$). ^{1}H NMR (DMSO): δ 13.21 (NH$_{Bz}$), δ 6.49–8.50 (8H, m, aromatic protons), δ 6.78 (NH$_{sec}$) and δ 4.98 & 5.27 (CH$_2$). UV/vis. (DMF): 270, 279, and 292 nm. Molar Cond. (10^{-3} M, DMF): 14.84 Ω^{-1} cm^2 mol^{-1}.

2.1.3. Data for **Pd–L (X = Br) (2)** ($C_{14}H_{20}Br_3N_3O_4Pd$)

Color: Yellow. Yield: 82%. MS: m/z = 301, 220, 131 and 118. Anal. Calcd. %C, 26.25; %H, 3.15; %N, 6.56; %Pd, 16.62. Found: %C, 26.22; %H, 3.19; %N, 6.76; %Pd, 16.52. FT-IR: 3416 (ν(NH)$_{sec}$), 1446 (ν(NH$_b$)$_{sec}$), 1318 (ν(C–N)$_{Bz}$), 1280 (ν(C–N)$_{sec}$), 612 (ρ_w(OH$_2$)), and 512 (ρ_t(OH$_2$)). ^{1}H NMR (DMSO): δ 13.21 (NH$_{Bz}$), δ 6.65–8.46 (8H, m, aromatic protons), δ 6.87 (NH$_{sec}$) and δ 5.09 & 5.31 (CH$_2$). UV/vis. (DMF): 270, 280, and 293 nm. Molar Cond. (10^{-3} M, DMF): 57.50 Ω^{-1} cm^2 mol^{-1}.

2.1.4. Data for **Pd–L (X = I) (3)** ($C_{14}H_{20}BrI_2N_3O_4Pd$)

Color: Blue-Black. Yield: 78%. MS: m/z = 346, 301, 220, 173, 131, 118 and 91. Anal. Calcd. %C, 22.89; %H, 2.74; %N, 5.72; %Pd, 14.49. Found: %C, 22.87; %H, 2.68; %N, 5.76; %Pd, 14.43. FT-IR: 3419 (ν(NH)$_{sec}$), 3274 (ν(NH)$_{Bz}$), 1655 (ν(C=N)), 1456 (ν(NH$_b$)$_{sec}$),1305 (ν(C–N)$_{sec}$) and 619 (ρ_w(OH$_2$)). ^{1}H NMR (DMSO): δ 13.20 (NH$_{Bz}$), δ 6.62–8.32 (8H, m, aromatic protons), δ 6.81 (NH$_{sec}$) and δ 4.74 & 5.17 (CH$_2$). UV/vis. (DMF): 266, 280, 293, and 352 nm. Molar Cond. (10^{-3} M, DMF): 78.71 Ω^{-1} cm^2 mol^{-1}.

2.1.5. Data for **Pd–L (X = SCN) (4)** ($C_{16}H_{18}BrN_5O_3S_2Pd$)

Color: Orange yellow. Yield: 80%. MS: m/z = 301, 272, 219, 172, 131, 118 and 91. Anal. Calcd. %C, 32.20; %H, 3.38; %N, 11.73; %Pd, 17.83. Found: %C, 32.01; %H, 3.41; %N, 11.72; %Pd, 17.77. FT-IR: 3415 (ν(NH)$_{sec}$), 2110 (ν(C≡N)), 1657 (ν(C=N)), 1457 (ν(NH$_b$)$_{sec}$),1307 (ν(C–N)$_{sec}$), 914 (ν(C=S)), 850 (ρ_r(OH$_2$)), 641 (ρ_w(OH$_2$)), and 501 (ρ_t(OH$_2$)). ^{1}H NMR (DMSO): δ 13.48 (NH$_{Bz}$), δ 6.61–8.39 (8H, m, aromatic protons), δ 6.91 (NH$_{sec}$) and δ 5.17 (CH$_2$). UV/vis. (DMF): 269, 279, and 297 nm. Molar Cond. (10^{-3} M, DMF): 90.42 Ω^{-1} cm^2 mol^{-1}.

2.1.6. Data for **Pd–L (X = NO_3) (5)** ($C_{14}H_{16}BrN_5O_8Pd$)

Color: Grey-green. Yield: 83%. MS: m/z = 301, 220, 131 and 118. Anal. Calcd. %C, 29.57; %H, 2.84; %N, 12.32; %Pd, 18.72. Found: %C, 29.50; %H, 2.77; %N, 12.23; %Pd, 18.60. FT-IR: 3438 (ν(NH)$_{sec}$), 1602 (ν(C=N)), 1483 (ν_{as}(NO)), 1445 (ν(NH$_b$)$_{sec}$), 1321 (ν(C–N)$_{Bz}$), 1281 (ν(C–N)$_{sec}$), 934 (ν(NO)), 614 (ρ_w(OH$_2$)), and 517 (ρ_t(OH$_2$)). ^{1}H NMR (DMSO): δ 13.25 (NH$_{Bz}$), δ 6.63–9.00 (8H, m, aromatic protons), δ 6.92 (NH$_{sec}$) and δ 4.95 & 5.21 (CH$_2$). Uv/vis. (DMF): 270, 280, and 294 nm. Molar Cond. (10^{-3} M, DMF): 45.20 Ω^{-1} cm^2 mol^{-1}.

2.1.7. Data for **Pt–L (X = Cl) (6)** ($C_{14}H_{12}BrCl_2N_3Pt$)

Color: Brown. Yield: 71%. MS: m/z = 405, 382, 365, 350, 323, 301, 287, 259, 244, 210, 171, 131, 118 and 91. Anal. Calcd. %C, 29.60; %H, 2.13; %N, 7.40; %Pt, 34.34. Found: %C, 29.82; %H, 2.09; %N, 7.36; %Pt, 34.29. FT-IR: 3406 (ν(NH)$_{sec}$), 1670 (ν(C=N)), 1450 (ν(NH$_b$)$_{sec}$), 1339 (ν(C–N)$_{Bz}$), and 1281 (ν(C–N)$_{sec}$). ^{1}H NMR (DMSO): δ 13.44 (NH$_{Bz}$), δ 6.97–8.70 (8H, m, aromatic protons), δ 7.21 (NH$_{sec}$) and δ 4.83 & 4.96 (CH$_2$). Uv/vis. (DMF): 273, 280, 362, and 419 nm. Molar Cond. (10^{-3} M, DMF): 15.18 Ω^{-1} cm^2 mol^{-1}.

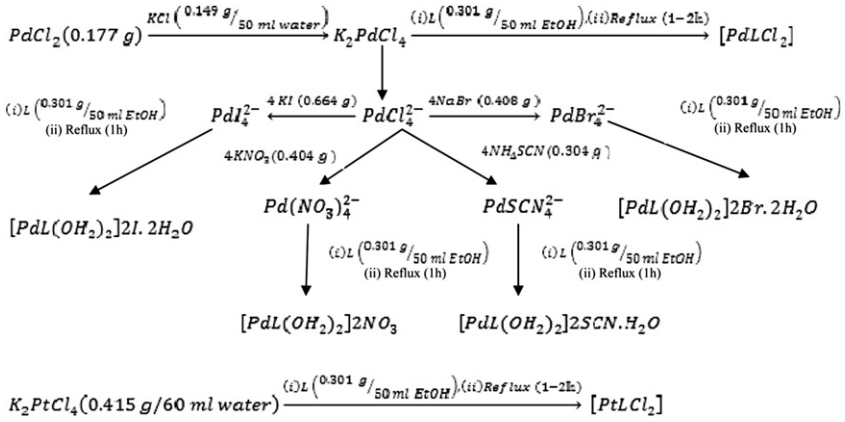

Scheme 1. Synthetic procedures for the Pd–L (**1**–**5**) and Pt–L (**6**) complexes.

2.2. Instruments

Infrared spectra of the ligand and its complexes were recorded in potassium bromide discs using *FTIR-460 plus, JASCO*, in 4000-200 cm^{-1} region. The ^1H NMR spectra were run at 300 MHz in DMSO-d_6 using *Varian-Oxford Mercury VX-300 NMR*. The mass spectra were recorded with the aid of a *SHIMADZU QP-2010 plus mass spectrometer* at 70 eV. The X-ray powder diffraction patterns were recorded over $2\theta = 5–60^\circ$ range using Philips X-ray diffractometer model PW 1840. Radiation was provided by copper anode (K_α, $\lambda = 1.54056$ Å) operated at 40 kV and 25 mA. The thermal analyses (TG/DTA) were carried out in a dynamic nitrogen atmosphere (20 ml min^{-1}) with a heating rate of 10 °C min^{-1} in a platinum crucible using *DTG-60H SIMULTANEOUS DTA-TG APPARATUS-SHIMADZU*. The UV/vis. measurements were carried out using automated spectrophotometer UV/vis. *SHIMADZU Lambda 4B* using 1 cm matched quartz cells. Elemental micro-analyses were performed at the Micro-analytical Center, Cairo University. The analyses were repeated twice to check the accuracy of the analyzed data. The metal content was determined gravimetrically [9]. Digital *Jenway 4330* Conductivity-pH meter with (1.02) cell constant was used for pH and molar conductance measurements.

2.3. X-ray crystallography

The single crystals of the benzimidazole L were grown by slow evaporation of its ethanolic solution at room temperature over a period of one month. The crystallographic analysis was carried out on an Enraf–Nonius CAD4 diffractometer, using graphite monochromated Mo-K_α radiation (k = 0.71069 Å) at room temperature. Three standard reflections were monitored during data collection and no significant intensity decay was observed. All diffracted intensities were corrected for Lorentz and polarization effects [10,11]. The structure was solved by direct methods and was refined by the full-matrix least-squares method using *SIR*92 [12] computer programs in the space group $P2_1/c$. All diagrams and calculations were performed using maXus [13], while the molecular graphics were given using *ORTEP* (Johnson, 1976). The figures involving Hydrogen bonds and packing were drawn using Mercury [14]. Further relevant crystallographic data are summarized (supplementary material, table S1).

2.4. Theoretical calculations

The molecular structure of the benzimidazole ligand in the ground state was optimized by a DFT/B3LYP method [15] using 6–31G(d) and LANL2DZ basis sets. Calculations were carried out by *GAUSSIAN03* [16] suite of programs. The optimized geometry was verified by performing a frequency calculation. Vibrational modes were analyzed using *GAUSSVIEW* software [17]. The main reason for choosing the LANL2DZ basis set is its inclusion of relativistic effect that is essential for heavy elements e.g. Pd(II) and Pt(II), in order to compare between the optimized structures of the ligand and its complexes. The ^1H NMR chemical shifts of compound L were computed at the B3LYP/6-311+G(2d,p) level of theory in the gaseous state by applying GIAO approach [18] and the values for the ^1H-isotropic were referenced to TMS, which was calculated at the same level of theory. The gas phase geometries of the studied complexes were optimized by B3LYP/LANL2DZ method. Net atomic charges had been obtained using the natural bond orbital (NBO) analysis of Weinhold and Carpenter. Frontier molecular orbitals (FMO) were performed at the same level of theory.

2.5. Biological activity

2.5.1. Antimicrobial activity

The antimicrobial activities of the test samples were determined by a modified *Kirby–Bauer disc diffusion method* [19] under standard conditions using *Mueller-Hinton* agar medium (tested for composition and pH), as described by NCCLS [20]. The antimicrobial activities were carried out using culture of *Bacillus subtilis*, *Staphylococcus aureus,* and *Streptococcus faecalis* as Gram-positive bacteria and *Escherichia coli*, *Pseudomonas aeruginoca*, and *Neisseria gonorrhea* as Gram-negative bacteria. The solution of 100 mg/ml of each compound (free ligand, metal complexes and standard drug *Tetracycline*) in DMSO was prepared for testing. Centrifuged pellets of bacteria from a 24 h old culture containing approximately $10^4–10^6$ CFU/ml (colony forming unit) were spread on the surface of *Mueller Hinton* Agar plates. Then the wells were seeded with 10 ml of prepared inocula to have 10^6 CFU/ml. Petri plates were prepared by pouring 100 ml of seeded nutrient agar. DMSO (0.1 ml) alone was used as control under the same conditions for each microorganism, subtracting the diameter of inhibition zone resulting with DMSO, from that obtained in each case. The antimicrobial activities could be calculated as a mean of three replicates.

2.5.2. Anticancer activity

Three human cancer cell lines were used for *in vitro* screening experiments; *breast cancer* (MCF7), *colon carcinoma* (HCT) and *human heptaocellular carcinoma* ($HepG_2$). They were obtained frozen in liquid nitrogen (−180 °C) from the American Type Culture

Collection. The tumor cell lines were maintained in the National Cancer Institute, Cairo, Egypt, by serial sub-culturing. Potential cytotoxicity of the compounds was tested using Skehan et al. method [21]. Cells were plated in 96-multiwell plate (5×10^3–4×10^4 cells/well) for 24 h before treatment with the compounds to allow the attachment of cell to the wall of the plate. RPMI-1640 medium (5% fetal bovine serum and 2 mM L-glutamine) was used for culturing and maintenance of the human tumor cell lines [22]. Different concentrations (50 and 100 μM) of the compounds under study were added to the cell monolayer triplicate wells were prepared for each individual dose. The monolayer cells were incubated with the compounds for 48 h at 37 °C and in 5% CO_2 atmosphere. After 48 h, cells were fixed, washed, and stained with the protein-binding dye sulforhodamine B (SRB) [20]. Excess stain was washed with acetic acid and attached stain was recovered with tris–EDTA buffer. The optical density (O.D.) of each well was measured spectro-photometrically at 564 nm with an ELIZA microplate reader and the mean background absorbance was automatically subtracted and mean values of each drug concentration was calculated. The relation between surviving fraction and drug concentration is plotted to get the survival curve. The results were compared with a similar run of *cis-platin* as an antitumor compound.

3. Results and discussion

3.1. IR spectral studies

The theoretical IR spectra of the benzimidazole (L) were obtained at DFT/B3LYP level of theory using 6–31G(d) and LANL2DZ basis sets. At this level, the calculated harmonic force constants and frequencies are higher than the corresponding experimental quantities, due to basis set truncation and neglecting of electron correlation and mechanical anharmonicity [23]. To compensate these shortcomings, scale factors were introduced and an explanation of this approach was discussed [24]. Two different methods were applied: **(i)** *uniform* scaling [24], the scaling factors are 0.963 for 6–31G(d) and 0.970 for LANL2DZ basis set **(ii)** *linear regression method* [25]; in this method, the plot of the calculated frequencies versus their experimental values resulted in a straight line, whose equation was used to correct the calculated frequencies (ν_{calc}).

The benzimidazole L has a strong intermolecular hydrogen bond, N9–H…N8, which makes the IR spectrum shows a broad band in the region 3500–2200 cm^{-1} and thus it is difficult to assign the $\nu(NH_{Bz})$ mode. By using B3LYP/6–31G(d) method, the scaled calculated value at 3513 cm^{-1} is assigned to the $\nu(NH_{Bz})$. This group is still masked in the studied metal complexes owing to the hydrogen bond effect generated by water molecules, whereas complex **(3)** has a sharp band at 3274 cm^{-1} [5]. In addition, the theoretically scaled $\nu(NH_{Bz})$ in the free ligand and its complexes is found at the same position, 3570 cm^{-1} (calculated by B3LYP/LANL2DZ), confirming that the NH_{Bz} group remains intact in the complexes as found experimentally.

The sharp band at 3445 cm^{-1} in the benzimidazole L is assigned to $\nu(NH_{sec})$ with deviation of 18 cm^{-1} from the theoretically scaled value (supplementary material, table S2). This discrepancy may be justified on the basis that the calculations were performed on a single molecule in the gaseous state contrary to the experimental values, which were recorded in presence of intermolecular interactions. This band is still observed in the complexes, but it is shifted to lower frequency (3438–3406 cm^{-1}) and becomes broad, indicating its involvement in the coordination sphere. The ν(C=N) mode in the free ligand is overlapped with the ν(C=C) vibrations in the same region due to the effect of hydrogen bond, whereas its theoretical value is found at 1683 cm^{-1} [26]. In complexes, the C=N group is liberated from the effect of hydrogen bonding with increasing of the double bond character and is observed in the 1670-1602 cm^{-1} range. This also confirms the participation of the pyridine-type nitrogen in the coordination sphere.

The IR spectrum of the Pd-L (X = SCN) **(4)** displays ν(C≡N) as strong band at 2110 cm^{-1}. This value is higher than that of N-bonded and S-bonded complexes [27], indicating the absence of SCN group in the first coordination sphere as confirmed by the disappearance of M-N or M-S stretching modes and its conductance value. The nitrato palladium complex **(5)** shows two bands at 1483 and 934 cm^{-1} due to $\nu(NO_2)_{asy}$ and ν(NO), respectively [27]. The IR spectra of complexes **(2-5)** showed the librational modes of water [27] e.g. the thiocyanate complex **(4)** exhibits the librational modes (rocking (ρ_r), twisting (ρ_t) and wagging (ρ_w)) at 850, 641 and 501 cm^{-1}, respectively.

The far-IR spectra of the palladium complexes (X = Cl, Br or I) **(1–3)** show two medium bands at 369 and 363 cm^{-1} for Pd-L (X = Cl) **(1)**, which are assigned to ν(Pd–Cl) in a cis-square planar structure [25]. Similar, the Pt-L complex **(6)** shows these modes at 367 and 355 cm^{-1}. Theoretically, the bands at 331 and 325 cm^{-1} are assigned to ν_{ss}(Pd–Cl) and ν_{ass}(Pd–Cl) modes, respectively, while the scissoring bending mode of Cl–Pd–Cl is found at 128 cm^{-1}. For Pt-L complex **(6)**, the scaled ν_{ss}(Pt–Cl), ν_{ass}(Pt–Cl) and the scissoring Cl–Pt–Cl modes are established at 324, 319 and 143 cm^{-1}, respectively. Moreover, the theoretically scaled vibrations at 290 and 264 cm^{-1} in the Pd-L complex **(1)** are assigned to $\nu(Pd–N_{py})$ and $\nu(Pd–NH_{sec})$, while the bands at 283 and 237 cm^{-1} are allocated for $\nu(Pt–N_{py})$ and $\nu(Pt–NH_{sec})$ in the Pt–L complex **(6)**. The RMS error of the frequencies between the un-scaled and experimentally values in the benzimidazole L was found to be 73 cm^{-1}. After scaling, the RMS error are found to be 8 and 25 cm^{-1} for 6–31G(d) and LANL2DZ basis sets, respectively, suggesting that the 6–31G(d) basis set gives more accurate results. Finally, FT-IR study revealed that the ligand is coordinated to the metal ions *via* the pyridine-type nitrogen (N_{py}) and the secondary amino group (NH_{sec}).

3.2. ^1H NMR studies

The δ NH_{Bz} signal appears at 12.27 ppm [28] in the benzimidazole L and moves downfield in its complexes (13.20–13.48 ppm). This shift is related to the charge density change in the benzimidazole ring, which supports the fact that the coordination occurs *via* the pyridine-type nitrogen. The triplet signal at 6.50 ppm is due to the NH_{sec} group, whereas the doublet signal at 4.46 ppm is assigned to the CH_2 group (supplementary material, figure S1). In complexes, both signals move downfield owing to the participation of the NH_{sec} group in the chelation. The methylene group appears as a pair of quartet between 4.74 and 5.31 ppm in the complexes, as the CH_2 protons are no longer isochronous, where the equatorial proton points away from the metal ion than the axial one does.

The protons of the aniline ring give rise to four-line pattern at 6.60, 6.63 ppm for the two protons in the ortho-position with respect to NH_{sec} and 7.19, 7.22 ppm regarding to the bromine atom. However, the signals of the benzimidazole protons are much broader and are shown at 7.12, 7.14, 7.48, and 7.50 ppm. In complexes, the aromatic protons nearest the coordination centers are found to suffer maximum downfield shifts comparing to the other aromatic protons.

The calculated chemical shift of the methylene group (4.43 ppm) in the benzimidazole (L) is in a good agreement with the experimental value. The theoretical chemical shifts at 7.53, 7.45, 7.00, and 6.37 ppm are assigned to the aromatic protons of the aniline moiety, while the signals at 8.15, 7.63, 7.61, and 7.59 ppm are attributed to the benzimidazolic protons. Thus, the experimental

chemical shifts are slightly smaller than the calculated values. On the other hand, the calculated chemical shift of NH_{sec} group is smaller than that observed by 0.88 ppm, while that of the hydrogen-bonded proton (H9) is lower than the calculated one by 4.10 ppm [29]. These may be due to neglect of the non-specific solute–solvent interactions (in the gas phase), and the intermolecular hydrogen bond in our calculations as compared with the experimental chemical shifts that are obtained from the DMSO solutions (hydrogen-bonded solvent).

3.3. Mass spectrometry

The electron impact mass spectra of the ligand L and its complexes were recorded at 70 eV. The benzimidazole L has a molecular ion peak at m/z 302, and decomposes to offer a peak at m/z 131, which is assigned to 2-methylene benzimidazole and a fragment at m/z 171 due to 4-bromo-aniline. The mass spectrum of Pd-L complex **(1)** gives rise to M^+ at m/z = 478 due to $[PdLCl_2]^+$. Fragmentation pattern of this complex goes under three fragmentation routes as illustrated in Scheme 2. It was found that the participation of $C{=}N_{py}$ group in the coordination sphere introduces a weakness point through which the benzimidazole ring decomposes to imidazole moiety with a peak at m/z 241 due to [Pd(imidazole)Cl_2]$^+$.

Unfortunately, the mass spectra of the Pd-L complexes (X = Br, I, SCN & NO_3) **(2–5)** did not show the molecular ion peaks comparing to the palladium chloride complex **(1)**. This behavior reflects the lower stability of these complexes. The mass spectra of the Pd–L (X = Br & NO_3) complexes are typical as the ligand itself with fragments at m/z 301, 220, 131 and 118. However, the Pd–L (X = I) complex showed the latter fragments with two additional peaks at m/z 173 and 346, which are assigned to $[Pd(imidazole)]^{2+}$ and $[Pd(L{-}Br)(OH_2)]^{2+}$, respectively. Also, the Pd-L (X = SCN) complex displayed two additional fragments at m/z 173 and 272. The peak at m/z 272 is assigned to $[Pd(benzimidazole{-}CH_2)(OH_2)_2]^{2+}$. These fragments confirm the presence of water molecules in the coordination sphere of the studied complexes **(2-5)**.

The mass spectrum of the platinum complex **(6)** shows three fragmentation routes. The first route results in the appearance of a fragment at m/z 382 due to [Pt(Benzimidazole)Cl_2]. The 2nd dissociation step involves the loss of Br, Cl and $2C_2H_2$ (from the benzimidazole ring) from M^+ as in Pd–L **(1)** complex and gives a fragment at m/z 405. Further fragmentation occurs by the exclusion of one chlorine atom from the latter fragment to offer a peak at m/z 365, followed by the elimination of the imidazolic NH_{Bz} group to provide the second abundant fragment at m/z 350. The 3rd route involves the removal of $PtCl_2$ to give a fragment at m/z 301 due to ligand, which decomposed as the free ligand itself.

3.4. Electronic absorption

The electronic spectrum of the benzimidazole L displayed five absorption bands in ethanol at 206, 225, 249, 273 and 280 nm. The first two bands may be assigned to medium and low energy π-π^* transitions within the phenyl rings of the aniline and benzimidazole moieties, respectively [30]. In benzimidazole ring, three kinds of transitions are possible: (i) n–π^*, (ii) π–π^*, and (iii) charge-transfer. However, it is well established that the n–π^* transition is not observed in the benzimidazole compounds, although the system has a lone pair of electrons on the tertiary nitrogen atom [31]. Therefore, the remaining bands at 249, 273, and 280 nm may be assigned to π-π^* transitions in the benzimidazole ring. In addition, the bands at 273 and 280 nm appear doublet due to the presence of a tautomeric structure [32]. This phenomenon is supported by comparing our spectrum with the spectrum of 1-methyl-2-phenyl-benzimidazole [31], where this fine structure is lost.

The electronic spectra of 10^{-4} M of the complexes were scanned in DMF, where the two bands at 270 and 280 nm

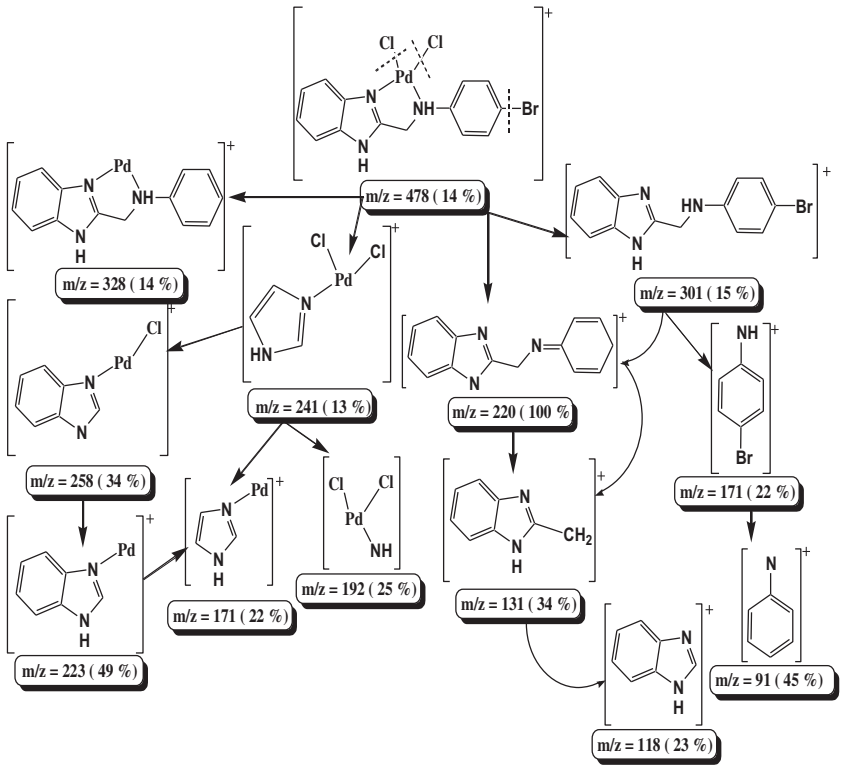

Scheme 2. Fragmentation pattern of Pd–L (X = Cl) **(1)** complex.

(35,714–37,000 cm^{-1}) are assigned to the internal ligand transitions (π-π^* in benzimidazole ring). The first low energy spin allowed band at 23,696 cm^{-1} (log $\varepsilon_{max} = 3.51$) in Pt-L complex **(6)** is assigned to the transition $b_{2g}(d_{xy}) - d_{1g}(d_{x^2-y^2})$ *i.e.* $^1A_{1g} \rightarrow {}^1A_{2g}$ (ν_1), comparable to the transition assigned by Jorgensen [33], for $PtCl_4^{2-}$ (21,500 cm^{-1}). This blue shift is ascribed to the stereochemical difference between the benzimidazole L and the chloride ion. The bands at 28,089 (log $\varepsilon_{max} = 3.50$) and 27,624 cm^{-1} (log $\varepsilon_{max} = 3.40$) in Pd–L **(3)** (X = I), and Pt-L **(6)** complexes, respectively, are assignable to a combination of $e_g(d_{yz}, d_{zx}) - b_{1g}(d_{x^2-y^2})$ *i.e.* $^1A_{1g} \rightarrow {}^1E_g$ bands (ν_3) and MLCT indicating a square planar geometry [34]. Other palladium complexes show only transitions corresponding to MLCT.

3.5. Thermal analyses and kinetics studies

Discussing the simultaneous TG/DTA curves constructed for Pd-L complex **(1)**, one can observe three endothermic mass loss stages at 310, 511, and 820 °C. The 1st decomposition step is accompanied by a mass loss, 23.37% (calcd. 23.60%) due to the exclusion of benzimidazole ring. The 2nd and 3rd stages are due to the loss of two chlorine atoms and N-methylene-4-bromoaniline with overall mass loss amounts to 73.58% (calcd. 75.31%) leaving Pd + C as a final residue [35]. The TG/DTA curves of Pt-L complex **(6)** resemble that found in Pd-L complex, with three endothermic peaks at 428, 495 and 807 °C. The overall weight loss amounts to 63.42% (calcd. 63.50%) with Pt metal as a final residue.

Examining the TG/DTA curves for Pd–L (X = Br, I, SCN and NO_3) **(2-5)** complexes, one can observe different degradation patterns. The thermogram of Pd–L (X = Br) complex **(2)** exhibits six endothermic distinct peaks at 55, 278, 346, 503, 599 and 758 °C. The 1st stage is responsible for desorption of two water molecules of hydration. The 2nd and 3rd thermal events are accompanied by a mass loss 30.57% (calcd. 30.53%) owing to the removal of two coordinated water molecules and bromine gas. The subsequent 4th, 5th and 6th stages are assigned to the degradation of one ligand molecule with mass loss 47.44% (calcd. 47.25%) leaving Pd metal as a final residue. For Pd–L (X = I) complex **(3)**, the TG/DTA curves show four endothermic peaks at 289, 417, 571 and 809 °C. The 1st decomposition step is assigned to the releasing of one iodide atom, while the 2nd thermal event is attributed to the removal of two water molecules of hydration and two coordinated water. The 3rd and 4th stages are assigned to the decomposition of one ligand molecule and another iodide atom confirming the participation of iodide in hydrogen bonding. The overall mass loss amounts to 85.63% (calcd. 85.54%) leaving Pd metal as a final residue.

For Pd–L (X = SCN) complex **(4)**, the degradation starts at 130 °C with three decomposition stages centered at 261, 370, 582 and 800 °C. The 1st degradation step is owing to the releasing of one water molecule of hydration, two coordinated water molecules and two thiocyanate counterions. The 2nd and 3rd decomposition stages are attributed to the degradation of one ligand molecule leaving Pd metal as a final residue with overall mass loss amounting to 81.50% (calcd. 81.56%).

The thermogram of Pd–L (X = NO_3) complex **(5)** shows no inflection below 150 °C and exhibits four endothermic peaks at 188, 309, 491, and 757 °C. The decomposition steps resembled that found in complex **(4)**, but the degradation was incomplete up to 1200 °C. The overall mass loss amounts to 70.53% (calcd. 81.31%) assuming that the formation of Pd metal as a final residue as no other palladium compounds are present at 1200 °C [36]. The rate of decomposition of most complexes is fast in air than that in nitrogen due to the oxidative nature of air, which facilitates the oxidative decomposition. The TG curve of Pd-L (X = NO_3) complex in air shows four degradation steps with overall mass loss amounting to 81.11%.

The kinetic parameters were calculated using Coats–Redfern (CR) [37] and Horowitz–Metzger (HM) methods [38] and are tabulated in table (S3) (supplementary material, table S3). It was found that the studied complexes have negative entropy indicating that the complexes are formed spontaneously and are highly ordered in their activated states, while the positive ΔH^* values mean that the decomposition processes are endothermic.

3.6. X-ray crystallography

A view of the molecular structure of the benzimidazole L is shown in Fig. 1 and its selected crystallographic data are presented in Table 1. This compound crystallizes in a monoclinic space group $P2_1/c$. The cell packing is shown (supplementary material, figure S2). The crystal structure is deviated from planarity, where the angle (C10-C11-N12) between the aniline ring and benzimidazole moiety is 112.76°. This deviation is possibly caused by the intermolecular hydrogen bonding; N9-H…N8 with D-A distance of 2.003 Å. In addition, the benzimidazole L forms an infinite chain structure with a trans-zigzag type along the crystallographic axis "a", through this hydrogen bond (Fig. 2). A significant difference (0.035 Å) is found between the N8–C10 and N9–C10 bond lengths and this confirms that the hydrogen atom is fixed at one of the two nitrogen atoms through the hydrogen bonding. In addition, it is possible to observe π-π stacking interactions between the ring planes along the crystallographic axis "c" (Fig. 3). The bond angle N8-C10-N9 (112°) is close to that of 2-methyl benzimidazole (112.7°).

3.7. X-ray powder diffraction

The X-ray powder diffraction patterns of the benzimidazole L, Pd–L (X = Cl) **(1)**, Pd–L (X = SCN) **(4)** and Pt–L **(6)** complexes were recorded over $2\theta = 5–60°$ in order to obtain an idea about the lattice dynamics of these compounds. The values of 2θ, interplanar spacing d (Å) and the relative intensities (I/I^o) of benzimidazole L and its complexes were tabulated in Table 2. The comparison between the obtained XRD patterns of L and its complexes (supplementary material, figure S3), throws light on the fact that each complex represents a definite compound with a distinct structure. The identification of the complexes was done by the known method [39]. Such facts suggest that the Pd–L (X = Cl) **(1)** and Pd–L (X = SCN) **(4)** complexes are amorphous, while the Pt–L **(6)** complex is nano-crystalline [39]. The X-ray powder diffraction pattern of benzimidazole (L) shows three low-angle diffraction peaks (below 11.00°) that are not observed in the parent benzimidazole [40] with acceptable intensity. Several peaks characterized to the benzimidazole moiety are also observed at 18.52°, 19.77°, 31.80°, and 35.94°.

3.8. Theoretical calculations

3.8.1. Geometry optimization

Full geometry optimization of benzimidazole L was performed at the DFT level of theory [15]. As shown in Table 1, the relative errors in the calculated values are less than 2% by using 6–31G(d) basis set. Most of the optimized bond lengths are slightly longer than the experimental values agreeing within 0.007–0.026 Å except the N–C bonds (0.059 Å), while the bond angles are slightly different by 0.2–2.2° except the N–C–C angle (4.6°). This happens because the calculations were performed in the gaseous state, whereas packing molecules with intermolecular interactions are treated in the experimental measurements. Moreover, the

Table 1
Geometrical parameters optimized in benzimidazole L, crystallographic data (bond length (Å), bond angles (°) and charges), theoretically computed energies, zero-point vibrational energies, rotational constants, entropies and dipole moment.

Bond lengths (Å)	Exp.	B3LYP/6−31G(d)	B3LYP/LANL2DZ	Bond angles (°)	Exp.	B3LYP/6−31G(d)	B3LYP/LANL2DZ	Charge B3LYP/6−31G(d)
Br1C17	1.906	1.916	1.975	Br1C17C16	120.3	119.939	119.805	C1 = −0.143
C2C3	1.378	1.399	1.407	Br1C17C18	119.5	119.786	119.660	C2 = −0.148
C3C4	1.391	1.415	1.428	C2C3C4	122.7	119.874	120.163	C3 = −0.178
C4C5	1.388	1.395	1.404	C2C7C6	120.5	121.405	121.345	C4 = 0.239
C5C6	1.365	1.393	1.406	C3C2C7	117.3	117.956	117.862	C5 = 0.356
C6C7	1.411	1.409	1.421	C3C4C5	120.0	122.574	122.371	C6 = −0.175
C7C2	1.368	1.392	1.404	C7C6C5	122.1	121.556	121.543	C7 = 0.515
N8C3	1.391	1.391	1.411	C4C5C6	117.5	116.635	116.716	C8 = −0.155
N8C10	1.362	1.309	1.330	N8C3C4	105.4	110.117	109.661	C9 = 0.409
N9C4	1.380	1.388	1.404	N8C3C2	131.9	130.009	130.176	C10 = −0.189
N9C10	1.317	1.376	1.394	N9C4C3	109.4	104.469	104.833	C11 = −0.154
C10C11	1.490	1.503	1.506	N9C4C5	130.6	132.957	132.796	C12 = 0.075
N12C11	1.446	1.436	1.450	N8C10N9	112.0	113.051	112.327	C13 = −0.160
N12C14	1.379	1.374	1.387	C10N9C4	106.2	107.085	107.388	C14 = −0.193
C14C13	1.396	1.412	1.423	C10N8C3	106.9	105.278	105.790	N15 = −0.578
C18C13	1.384	1.388	1.401	N9N8C10	33.4	34.423	34.736	N16 = −0.750
C18C17	1.365	1.396	1.407	N8N9C10	34.7	32.526	32.936	N17 = −0.712
C17C16	1.386	1.390	1.401	N8C10C11	122.2	122.463	124.362	H18 = 0.142
C15C16	1.356	1.395	1.407	N9C10C11	125.9	124.486	123.311	H19 = 0.130
C15C14	1.405	1.409	1.421	C10C11N12	112.7	109.012	108.751	H20 = 0.131
N9H9	0.960	1.010	1.011	C14N12C11	123.4	124.423	106.162	H21 = 0.130
C5H5	0.960	1.086	1.087	N12C14C13	123.0	119.721	119.703	H22 = 0.333
C6H6	0.960	1.086	1.087	C15C14N12	120.7	122.218	122.102	H233 = 0.162
C7H7	0.960	1.087	1.087	C18C13C14	121.5	121.086	121.015	H24 = 0.162
N12H12	0.960	1.012	1.015	C18C17C16	120.2	120.275	120.535	H25 = 0.354
C11H11A	0.960	1.105	1.106	C14C15C16	122.3	120.737	120.728	H26 = 0.131
C11H11B	0.960	1.105	1.106	C15C14C13	116.3	118.061	118.195	H27 = 0.149
C13H13	0.960	1.087	1.088	C15C16C17	119.7	120.031	119.860	H28 = 0.146
C15H15	0.960	1.085	1.086	C13C18C17	119.9	119.811	119.667	H29 = 0.125
C16H16	0.960	1.085	1.086	C13C18H18	120.1	120.038	119.806	Br30 = -0.156
C18H18	0.960	1.085	1.086	C17C18H18	120.0	120.151	120.527	
N8N9	2.221	2.240	2.262	C14C15H15	119.8	120.456	120.652	
		B3LYP/6−31G(d)	B3LYP/LANL2DZ	C16C15H15	117.8	118.807	118.620	
				C14N12H12	119.5	120.292	120.891	
E (a.u.)		−718.690	−718.027	C11N12H12	117.1	115.275	115.302	
Zero-point E (kcal mol^{-1})		146.988	148.029	C18C13H13	119.9	119.594	119.475	
				C2C7H7	119.9	119.515	119.583	
Rotational constants (GHz)		2.001	1.965	C6C7H7	119.6	119.080	119.073	
		0.081	0.079					
		0.078	0.076	C15C16H16	120.4	119.860	119.656	
Entropy (cal mol^{-1} K^{-1})				C17C16H16	119.9	120.109	120.484	
				C3C2H2	119.1	120.322	120.454	
Translational		43.003	43.003	C4C5H5	120.7	122.046	122.262	
Rotational		34.495	34.555	C6C5H5	121.8	121.319	121.022	
Vibrational		46.718	49.477	C10C11H11A	108.4	109.316	109.429	
Total Dipole moment (D)		5.576	6.361	C10C11H11B	110.0	109.312	109.414	
				N12C11H11A	108.0	111.643	111.431	
				N12C11H11B	108.2	111.524	111.404	
				H11AC11H11B	109.5	105.970	106.371	
				C7C6H6	119.4	119.291	119.168	
				C5C6H6	118.6	119.153	119.288	

experimental bond lengths of X–H bonds are shorter than the estimated bond lengths owing to the low scattering factors of hydrogen atoms in X-ray diffraction. The benzimidazole L shows accumulation of the negative charge density on the pyridine-type nitrogen, which is a very important structural feature related directly to the ability to bind the metal ions. Several calculated thermodynamic parameters are presented in Table 1.

The fully optimized geometries of cis-$PdLCl_2$ and cis-$PtLCl_2$ and numbering of atoms are shown in Fig. 4. Some selected geometric parameters are listed in Table 3. The coordination sphere around the metallic center in these complexes is made up of N_{py}, NH_{sec} and 2Cl completing the square planar geometry. The four donor atoms are coplanar, while the phenyl ring is bent out of the coordination plane by angle 90.234° and 158.194° for $PdLCl_2$ and $PtLCl_2$ complexes, respectively. It was found that the M–NH_{sec} bond length is about 4.43% longer than the M–N_{py} bond distance (Table 3) [41]. It is seen that the optimized M–NH_{sec} and M–N_{py} bond lengths in the Pd–L complex are slightly longer than the Pt–NH_3 bond distance in cis-platin by 0.16 and 0.06 Å, respectively, while the M–Cl bond lengths are longer than Pt–Cl by 0.06 and 0.03 Å for M–Cl22 and M–Cl23, respectively, owing to the trans-effect. Finally, the Pd–N_{py} (2.071 Å) and Pd–NH_{sec} (2.172 Å) bond lengths are in agreement with that observed in some benzimidazole complexes [42]. For the Pt–L complex, the M–N bond lengths are shorter than that of the palladium complex by 0.02 Å.

The optimized N11–Pd–N21 (80.635°) is smaller than that of cis-platin (NH_3–Pt–NH_3) by 6.365°. This can be interpreted in terms of CH_2 group, which connects the two coordination sites and prevents opening of this angle. The calculated Cl22–Pd–Cl23 (95.005°) angle is larger than the experimental one in cis-platin molecule by 3.105° [43], since the intramolecular hydrogen bonding N21–H27…Cl22 (2.731 Å) opens up this angle. The

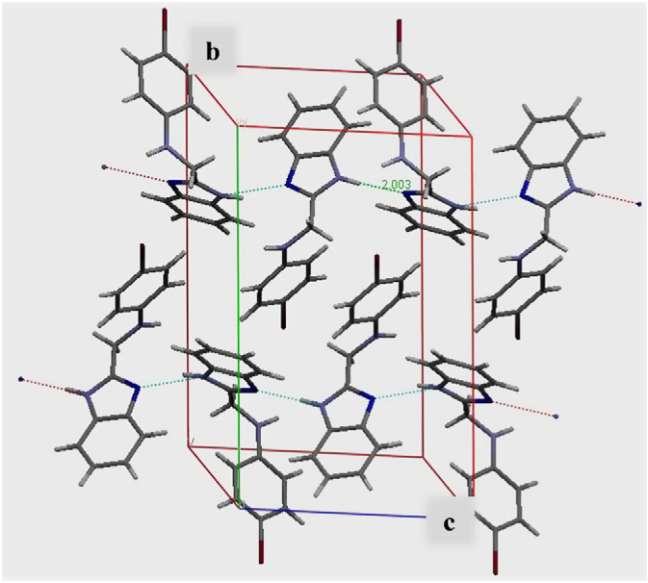

Fig. 2. Intermolecular hydrogen bonding stabilizing the crystal packing of benzimidazole L and forming zigzag infinite chain parallel to "a" axis.

optimized N11PtN21 is close to that found in cis–$PdLCl_2$ complex, while the Cl18PtC19 is slightly different from that exists in cis-platin by 1.5°. This indicates that there is a weak or almost no intramolecular hydrogen bonding as found in the cis–$PdLCl_2$ and this may be attributed to the significant difference in the bending angle of aniline ring as previously mentioned.

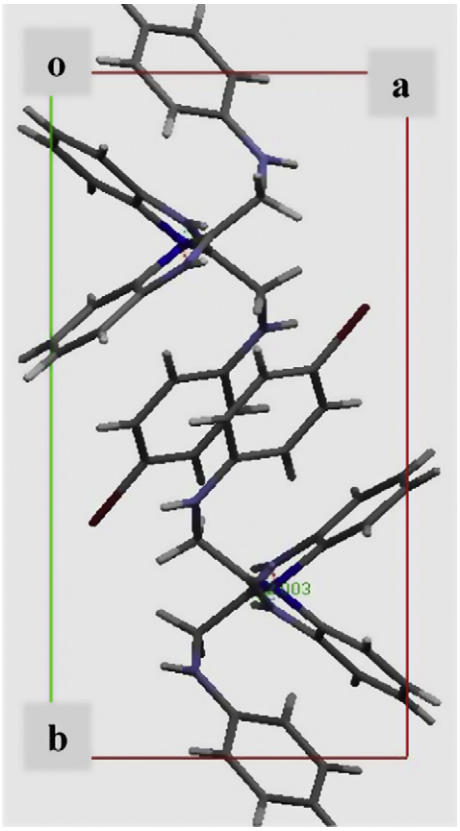

Fig. 3. A view along "c"-axis showing the π–π stacking interactions of benzimidazole L.

3.8.2. Natural bond orbital (NBO) analysis

The natural bond orbital (NBO) analysis of cis-$PtLCl_2$ complex was performed and can be used to estimate the delocalization of electron density between occupied Lewis-type orbitals and formally unoccupied non-Lewis NBOs (antibonding or Rydberg), which corresponds to a stabilizing donor–acceptor interaction [44]. Table 3 collects the natural charges on atoms. The largest negative charges are located on the two nitrogen atoms, N_{py} (−0.561 e) and NH_{sec} (−0.698 e). According to the NBO, the electron configuration of Pt is: [core]6 $s^{0.56}5d^{8.78}6p^{0.03}6d^{0.01}$. Thus, 68 core electrons, 9.34 valence electrons (on 6s and 5d atomic orbitals), and 0.04 Rydberg electrons (mainly on 6p, and 6d orbitals) give the 77.382 electrons. This is consistent with the calculated natural charge on Pt atom (+0.618e) in cis-$PtLCl_2$ complex, which corresponds to the difference between 77.382e and the total number of electrons in the isolated Pt atom (78e). In addition, the two chlorine atoms (Cl22 & Cl23) have larger negative charge −0.514e and −0.491e, respectively. Thus, the positive atomic charge upon the Pt(II) was substantially reduced as a consequence of electron density donation from 2Cl, N_{py} and NH_{sec}.

Table 4 lists the calculated occupancies of natural orbitals. Three classes of NBOs are included, the Lewis-type (s and p bonding or lone pair) orbitals, the valence non-Lewis (acceptors, formally unfilled) orbitals and the Rydberg NBOs, which originate from orbitals outside the atomic valence shell. The calculated natural hybrids on atoms are also given in this Table 4. According to calculations, the platinum atom forms two sigma bonds with two chlorine atoms, while the two bonds between platinum and the nitrogen atoms can be described as donation of electron density from a lone pair (LP) orbital on each nitrogen atom to platinum molecular orbitals. As follows from Table 4, the σ(Pt–Cl22) bond is formed from an $sp^{0.01}d^{1.19}$ hybrid on platinum atom (which is a mixture of 45.60% s, 0.30% p and 54.10% d atomic orbitals) and $sp^{8.94}$ hybrid on the chlorine atom (89.94% p contribution). Thus, the σ(Pt–Cl22) bond is strongly polarized towards the chlorine atom, with about 75.25% of electron density concentrated on the chlorine atom. The strength of this interaction can be estimated by the second order perturbation theory. Table 5 lists the selected values of the calculated second order interaction energy (E^2) between donor–acceptor orbitals in cis–$PtLCl_2$ complex. The strongest interactions are the electron donations from a lone pair orbital on the nitrogen atoms, LP(1)N11 to the antibonding acceptor σ*(Pt–Cl22) orbitals, e.g. LP(1)N11 → σ*(Pt–Cl22). As shown in Table 4, the LP(1)N11 orbital has 70.61% p-character and is occupied by 1.697 electrons (this is consistent with a delocalization of electron density from the idealized occupancy of 2.0 e). The donation of electron density from the coordination sites in the ligand to the Pt molecular orbitals has a clear correspondence to a chemical picture of the coordination bonds.

3.8.3. Frontier molecular orbitals

The frontier molecular orbitals play an important role in the electric and optical properties [45]. Fig. 5 shows the distributions and energy levels of the HOMO, and LUMO orbitals computed at the B3LYP/LANL2DZ level for cis-$PdLCl_2$ and cis-$PtLCl_2$ complexes. The value of the energy separation between the HOMO and LUMO is 4.952 and 3.864 eV for cis-$PdLCl_2$ and cis-$PtLCl_2$, respectively.

3.9. Structural interpretation

The structures of the Pd(II) (X = Cl, Br, I, SCN and NO_3) and Pt(II) (X = Cl) complexes are confirmed by spectral, TG/DTA, elemental analysis and molar conductance. FT-IR and ^{1}H NMR revealed that the benzimidazole L behaves as a neutral bidentate ligand through

Table 2
X-ray diffraction data of benzimidazole L, Pd–L (X = Cl) **(1)** and Pt–L **(6)** complexes.

L			Pd–L (X = Cl) (1)			Pt–L (6)		
Angle (2θ)	d-value (Å)	Relative intensity (I/I°) %	Angle (2θ)	d-value (Å)	Relative intensity (I/I°) %	Angle (2θ)	d-value (Å)	Relative intensity (I/I°) %
5.88	15.00	1.1	9.49	9.31	100	5.62	15.73	2.2
6.42	13.77	1.5	10.92	8.12	12.7	9.81	9.00	4.3
10.77	8.21	1.4	12.59	7.04	49.3	12.77	6.92	5.4
11.31	7.82	2.6	13.08	6.78	52	15.79	5.61	100
18.52	4.78	31.3	14.73	6.02	35.5	18.25	4.85	27.4
19.77	4.49	35.6	16.14	5.50	31.1	25.91	3.44	40.6
20.78	4.27	92.8	17.29	5.13	40.3	30.47	2.93	44.4
21.54	4.12	8.9	18.21	4.88	20.4	31.83	2.81	11.1
22.65	3.92	13.8	19.83	4.48	27.0	35.07	2.56	3.9
23.30	3.81	94.6	20.500	4.33	32.2	36.94	2.43	53.6
23.76	3.74	24.5	21.900	4.06	81.7	39.77	2.26	6.2
24.34	3.65	52.5	23.395	3.80	49.3	40.38	2.23	20.5
25.66	3.47	22.8	26.27	3.39	76.6	41.50	2.17	21.6
26.34	3.38	40.1	27.70	3.22	30	45.65	1.99	16.4
27.06	3.29	9.7	29.88	2.99	30	48.59	1.87	25.6
27.90	3.19	34.5	31.97	2.80	12	53.17	1.72	23.8
28.68	3.11	29.3	39.40	2.29	13.4	55.70	1.65	26.2
29.37	3.04	15.2	41.30	2.18	15.5	56.76	1.62	8.5
31.80	2.81	17.4						
32.43	2.76	13.5						
33.33	1.68	31.8						
34.14	2.62	21						
34.48	2.59	27.8						
35.94	2.49	30.3						
38.38	2.34	21.5						
39.76	2.26	16.7						
40.39	2.23	20.6						
42.13	2.14	20.6						
43.93	2.05	100						
45.95	1.97	28.3						
47.36	1.92	21.9						
48.96	1.85	32.4						
51.27	1.78	15.6						
53.94	1.69	17.4						
54.83	1.67	10.6						
57.35	1.61	6.8						

the pyridine-type nitrogen (N_{py}) of the benzimidazole ring and the secondary amino group (NH_{sec}). The Pd(II) and Pt(II) (X = Cl) complexes are non-electrolytes, while the Pd(II) complexes (X = Br, I, SCN or NO_3) are ionic. On the basis of the above observations, square planar geometry is suggested for the studied complexes with the general formula; $[MCl_2]$ (M = Pd and Pt) and $[PdL(OH_2)_2]\cdot 2X\cdot zH_2O$ (X = Br, I, z = 2; X = SCN, z = 1; X = NO_3, z = 0).

3.10. Biological activity

3.10.1. Antimicrobial activity

The antimicrobial activities of the studied ligand and its complexes were carried out using culture of *B. subtilis*, *S. aureus*, and *S. faecalis* as gram-positive bacteria and *E. coli*, *P. aeroginosa*, and *N. gonorrhea* as gram-negative bacteria. The data showed that

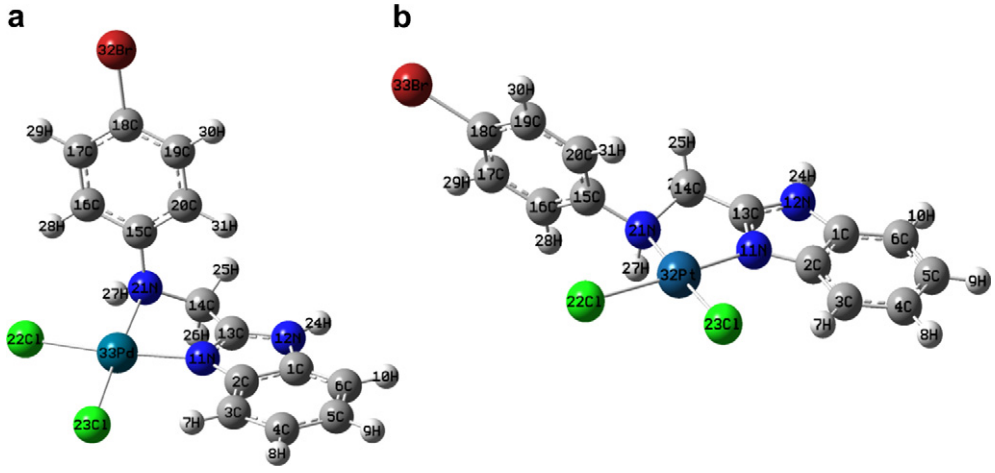

Fig. 4. Optimized structures of (a) Pd–L (1) (b) Pt–L **(6)** complexes.

Table 3
Selected bond lengths (Å), angles (°) and charge for Pd–L (X = Cl) **(1)** and Pt–L **(6)**.

Pd–L (X = Cl)					Pt–L				
Bond lengths (Å)		Bond angles (°)		Charge	Bond lengths (Å)		Bond angles (°)		Charge
C1C2	1.425	C1C2C3	121.002	C1 = 0.151	C1C2	1.425	C1C2C3	120.746	C1 = 0.154
C2C3	1.406	C2C3C4	116.984	C2 = 0.149	C2C3	1.407	C2C3C4	117.071	C2 = 0.149
C3C4	1.402	C3C4C5	121.745	C3 = −0.187	C3C4	1.402	C3C4C5	121.846	C3 = −0.186
C4C5	1.422	C4C5C6	121.655	C4 = −0.213	C4C5	1.421	C4C5C6	121.507	C4 = −0.213
C5C6	1.404	C5C6C1	116.479	C5 = −0.197	C5C6	1.404	C5C6C1	116.510	C5 = −0.197
C2N11	1.409	C6C1C2	122.135	C6 = −0.250	C2N11	1.415	C6C1C2	122.321	C6 = −0.251
C1N12	1.410	C2N11C13	107.554	N11 = −0.561	C1N12	1.409	C2N11C13	107.344	N11 = −0.561
C13N11	1.337	C1N12C13	107.670	N12 = −0.603	C13N11	1.338	C1N12C13	107.686	N12 = −0.598
C13N12	1.378	N11C13N12	111.185	C13 = 0.471	C13N12	1.376	N11C13N12	111.342	C13 = 0.471
C13C14	1.505	C13C14N21	108.500	C14 = −0.252	C13C14	1.496	C13C14N21	108.701	C14 = −0.243
C14N21	1.502	C14N21C15	117.007	C15 = 0.162	C14N21	1.523	C14N21C15	110.763	C15 = 0.163
C15N21	1.463	N21C15C16	118.262	C16 = −0.208	C15N21	1.477	N21C15C16	119.490	C16 = −0.225
C15C16	1.410	C15C16C17	120.045	C17 = −0.204	C15C16	1.403	C15C16C17	119.937	C17 = −0.212
C16C17	1.403	C16C17C18	119.559	C18 = −0.113	C16C17	1.408	C16C17C18	119.008	C18 = −0.106
C17C18	1.405	C17C18C19	120.856	C19 = −0.209	C17C18	1.403	C17C18C19	121.268	C19 = −0.204
C18C19	1.402	C18C19C20	119.518	C20 = −0.246	C18C19	1.406	C18C19C20	119.402	C20 = −0.205
C19C20	1.407	C19C20C15	120.040	N21 = −0.691	C19C20	1.403	C19C20C15	119.638	N21 = −0.698
C15C20	1.408	C20C15C16	119.975	Cl22 = −0.548	C15C20	1.405	C20C15C16	120.732	Cl22 = −0.514
N11Pd	2.071	N11PdN21	80.635	Cl23 = −0.499	N11Pt	2.054	N11PtN21	81.0518	Cl23 = −0.491
N21Pd	2.172	Cl22PdCl23	95.005	Pd = 0.686	N21Pt	2.152	Cl22PtCl23	90.456	Pt = 0.618
Cl22Pd	2.386				Cl22Pt	2.399			
Cl23Pd	2.366				Cl23Pt	2.395			
E (a.u.)			−874.774			−867.187			
Zero-point E (kcal mol^{-1})			151.793			151.792			
Rotational constants (GHz)			0.237, 0.097, 0.079			0.390, 0.074, 0.064			
Entropy (cal mol^{-1} K^{-1})									
Translational			44.374			44.885			
Rotational			36.421			36.406			
Vibrational			70.839			71.653			
Total Dipole moment (D)			14.602			15.607			

the ligand, Pd–L **(1)** and Pt–L **(6)** complexes have the capacity of inhibiting the metabolic growth of the investigated bacteria to different extents (Fig. 6). The benzimidazole L and its Pd–L **(1)** complex are toxic against the tested gram-positive bacteria, while the Pt–L complex is active only towards *B. subtilis*. For gram-negative bacteria, the tested ligand is active against these bacteria, while its Pd–L **(1)** complex shows toxicity only against the *N. Gonorrhea*. The Pt–L complex is inactive against the bacterium *E. coli*. The remarkable activity of these compounds may be arising from the benzimidazole ring, which may play an important role in the antibacterial activity. The mode of action may involve the formation of hydrogen bond through the pyridine-type nitrogen

Table 4
Occupancy of natural orbitals (NBOs) and hybrids calculated for Pt–L complex **(6)** (selected).

Donor[a] Lewis-type NBOs (A-B)	Occupancy	Hybrid[b]	AO (%)[c]	Acceptor[d] non-Lewis NBOs	NBOs
σ(C2–N11)	1.978	$sp^{1.86}$ (N11) $sp^{2.60}$ (C2)	s(35.02)p(64.98) s(27.82)p(72.18)	σ*(C2–N11)	0.036
σ(C13–N11)	1.978	$sp^{1.81}$ (N11) $sp^{2.14}$ (C13)	s(35.62)p(64.38) s(31.90)p(68.10)	σ*(C13–N11)	0.026
π(C13–N11)	1.899	sp (N11) $sp^{0.01}$ (C13)	p(100.00) s(0.01)p(99.99)	π*(C13–N11)	0.444
σ(C14–N21)	1.975	$sp^{2.92}$ (N21) $sp^{3.54}$(C14)	s(25.54)p(74.46) s(22.04)p(77.96)	σ*(Cl4–N21)	0.028
σ(C15–N21)	1.982	$sp^{2.02}$ (N21) $sp^{2.87}$(C15)	s(33.12)p(66.88) S(25.82)p(74.18)	σ*(C15–N21)	0.040
σ(Pt–Cl22)	1.966	$sp^{0.01}d^{1.19}$ (Pt) $sp^{8.94}$ (C122)	s(45.60)p(0.30)d(54.10) s(10.06)p(89.94)	σ*(Pt–Cl22)	0.313
σ(Pt–Cl23)	1.967	$sp^{0.01}d^{1.12}$ (Pt) $sp^{9.34}$ (C123)	s(46.95)p(0.35)d(52.70) s(9.67)p(90.33)	σ*(Pt–Cl23)	0.280
σ(N21–H27)	1.981	$sp^{3.05}$(N21)	s(24.71)p(75.29)		
LP(1)N11	1.697	$sp^{2.40}$	s(29.39)p(70.61)	RY*(1)N11	0.004
LP(1)N21	1.721	$sp^{5.01}$	s(16.63)p(83.37)	RY*(1)N21	0.0009
LP(1)Cl22	1.993	$sp^{0.25}$	s(79.89)p(20.11)	RY*(1)Cl22	0.0003
LP(1)Cl23	1.990	$sp^{0.25}$	s(79.83)p(20.17)	RY*(1)Cl23	0.0004
LP(1)Pt	1.993	$sp^{0.06}d^{49.02}$	s(2.00)p(0.13)d(97.88)	RY*(1)Pt	0.02
LP(2)Pt	1.986	$sp^{0.01}d^{20.08}$	s(4.74)p(0.07)d(95.19)	RY*(2)Pt	0.004
LP(3)Pt	1.980	$spd^{99.99}$	s(0.01)p(0.06)d(99.94)	RY*(3)Pt	0.002

[a] LP(n)A is a valence lone pair orbital (n) on A atom.
[b] Hybrid on A atom in the A–B bond or otherwise, as indicated.
[c] Percentage contribution of atomic orbitals in NBO hybrid.
[d] (*) denotes antibonding, and RY corresponds to the Rydberg NBO orbital.

Table 5
Second-order interaction energy (E^2, kcal/mol) between donor and acceptor orbitals in Pt-L **(6)** complex calculated at B3LYP/LANL2DZ level of theory (selected).

Donor → Acceptor	E^2	Donor → Acceptor	E^2
LP(1)N11 → σ*(Pt–Cl22)	98.49	σ(N21–H27) → σ*(Pt–Cl23)	5.95
LP(1)N21 → σ*(Pt–Cl23)	75.20	σ(Pt–Cl23) → σ*(Pt–Cl22)	4.79
σ(N11–C13) → σ*(Pt–Cl22)	6.08	σ(N21–C14) → σ*(Pt–Cl23)	2.91

with the active centers of the cell constituents, resulting in interference with the normal cell process.

A possible explanation for the poor activity of these complexes in comparison to the ligand L may be due to their inability to chelate metals essential for the metabolism of microorganisms and/or to form hydrogen bonds with the active centers of cell structures, resulting in an interference with the normal cell cycle. It is also due to their low lipophilicity, where the penetration of the complex through the lipid membrane is decreased and hence, they cannot block or inhibit the growth of the microorganism. Therefore, we confirm that the toxicity of the complexes can be related to the strengths of the M–L bond, in addition to other factors such as size of the cation, and receptor sites.

3.10.2. Anticancer activity

To evaluate the potential usefulness of the Pd(II) and Pt(II) complexes synthesized as antitumor agents, three cell lines of different origin *breast cancer* (MCF7), *colon carcinoma* (HCT) and *human hepatocarcinoma* ($HepG_2$) were treated. These experiments were performed at 50 and 100 μM and the results obtained were compared with that of cis-platin. As shown in Table 6, these complexes showed higher activity against the studied cell lines, especially $HepG_2$. The IC_{50} (the concentration that inhibited in 50% of the cellular proliferation) of these compounds and cis-platin were determined. According to Shier [46], the compounds exhibited IC_{50} activity within the range of 10–25 μg/ml are considered weak anticancer drugs, while those of IC_{50} activity between 5 and 10 μg/ml are moderate and compounds of activity below 5.00 μg/ml are considered strong agents.

The results showed that the activity of the studied compounds is higher than that of cis-platin at 100 μM on screening against $HepG_2$ cells. In addition, the palladium complexes are slightly affected by the nature of the anion and the inhibitory activity was found to be in decreasing order as follows: Cl **(1)** = Br **(2)** > SCN **(4)** > I **(3)** > NO_3 **(5)**. It was found that the Pd–L **(1)** complex possesses a moderate antitumor activity according to Shier scale with IC_{50} = 19.4 μM (equivalent to 9.27 μg/ml) comparing to that of cis-platin (IC_{50} = 11.9 μM, equivalent to 3.57 μg/ml) and is more toxic than the platinum complex **(6)**. The higher toxicity of Pd–L **(1)** complex than Pt–L **(6)** happens because the ligand-exchange behavior of platinum compound is quite slow, which gives them a high kinetic stability and results in ligand-exchange reactions of minutes to days, rather than microseconds to seconds for many other coordination compounds. In addition, another unusual phenomenon deals with the preferred ligands for platinum ions is that Pt(II) has a strong thermodynamic preference for binding to S-donor ligands and for this reason, one would predict that platinum compounds would perhaps never reach DNA, with many cellular platinophiles (S-donor ligands, such as glutathione, methionine) as competing ligands in the cytosol [47].

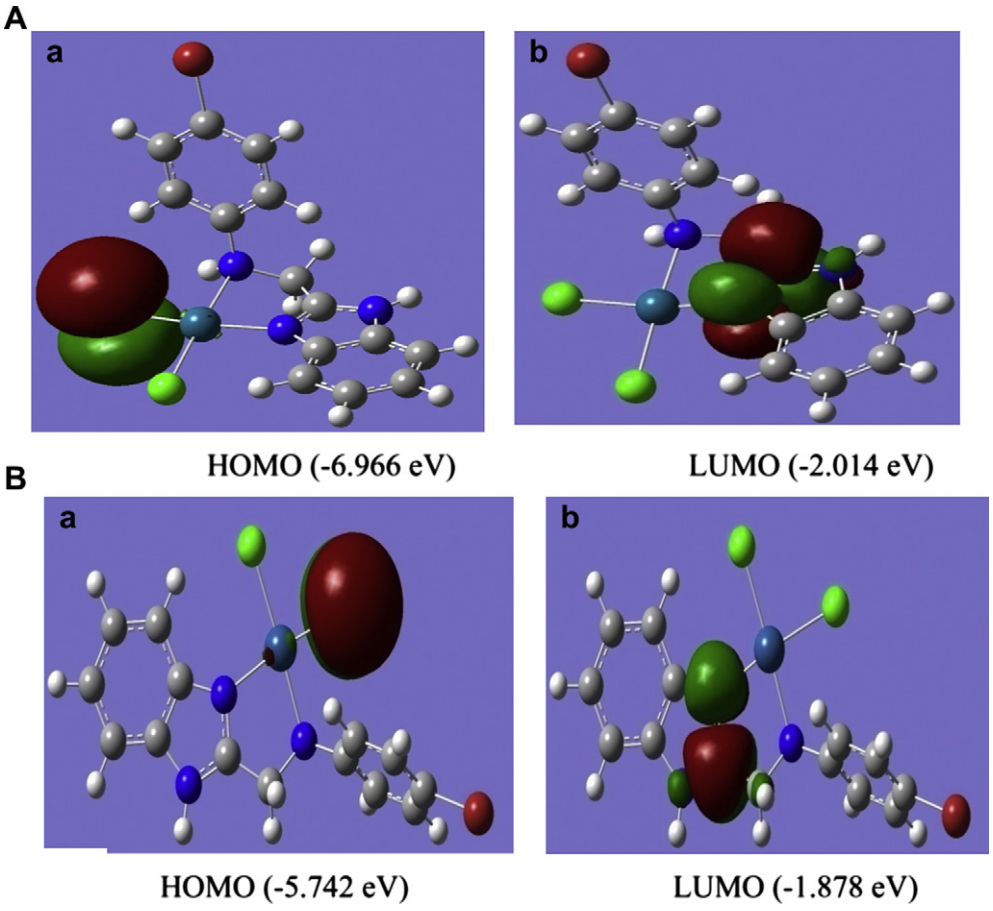

Fig. 5. Molecular orbital surfaces and energy levels of (A) Pd–L (**1**) (B) Pt–L **(6)**.

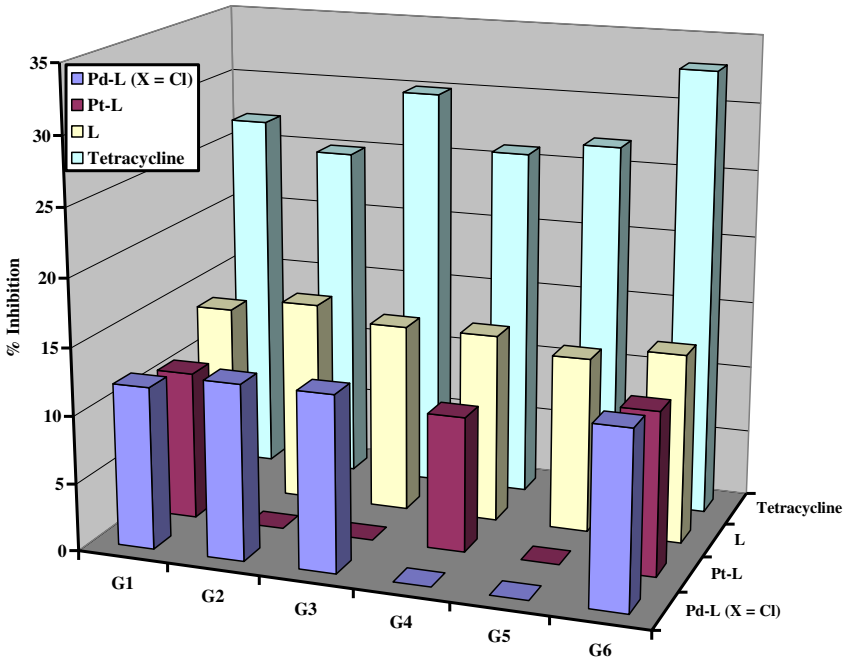

Fig. 6. Antibacterial activities of benzimidazole L and its complexes; Pd–L (X = Cl) **(1)** and Pt-L **(6)** against *B. subtilis* (G1), *S. aureus* (G2), *S. faecalis* (G3) as Gram-positive, *P. aeruginosa* (G4), *E. coli* (G5), *N. Gonorrhea* (G6) as Gram-negative bacteria. All experiments were carried out in triplicate and the mean results are given.

Table 6
The *in vitro* cytotoxicity effect of Pd(II) and Pt(II) complexes.

Compound	% Inhibition[a]					
	50 μM			100 μM		
	HCT	$HEPG_2$	MCF-7	HCT	$HEPG_2$	MCF-7
Pd–L (X = Cl) **(1)**	57 ± 1.82	52 ± 2.54	50 ± 1.37	70 ± 0.43	89 ± 1.30	78 ± 0.89
Pd–L (X = Br) **(2)**	54 ± 0.16	48 ± 1.35	58 ± 1.36	74 ± 0.25	89 ± 1.22	77 ± 0.61
Pd–L (X = I) **(3)**	52 ± 0.60	60 ± 1.05	40 ± 4.11	76 ± 1.38	85 ± 1.78	76 ± 1.86
Pd–L (X = SCN) **(4)**	44 ± 1.02	58 ± 1.15	36 ± 1.25	69 ± 2.78	86 ± 1.73	78 ± 1.67
Pd–L (X = NO_3) **(5)**	58 ± 4.22	60 ± 2.60	28 ± 1.25	77 ± 1.72	81 ± 2.24	76 ± 1.50
Pt–L **(6)**	58 ± 0.99	61 ± 2.27	33 ± 2.31	67 ± 1.43	82 ± 3.69	74 ± 2.65
Cis-plain	37 ± 1.25	30 ± 1.3	39 ± 1.89	58 ± 0.77	60 ± 1.2	67 ± 1.65

[a] Each value is the mean of six tests.

For palladium complexes, the cytotoxicity against MCF7 cell line decreases slightly in the sequence Cl **(1)** = SCN **(4)** > Br **(2)** > I **(3)** = NO_3 **(5)** and these complexes are more toxic than the platinum complex at the same concentration. Moreover, the platinum complex has a moderate antitumor activity with IC_{50} = 10.2 μM (5.78 μg/ml) comparing to that measured for cis-platin 9.91 μM (2.97, μg/ml). As shown in Table 6, the nitrato-palladium complex **(5)** was found to be the most cyctotoxic compound among the studied compounds towards the HCT cell line, while the platinum complex is the least one. The results obtained can be useful in understanding the factors that influence the activity of the complexes and in supporting the general assumption that the relationship between structure and activity is extremely complex.

4. Conclusion

Better approaches to the synthesis of the benzimidazole L and its complexes were developed. The comparisons of the DFT/B3LYP (6–31G(d) and LANL2DZ) calculations with the crystal structure and the vibrational and NMR spectra of the benzimidazole L showed excellent agreement. The inclusion of solvation to the ^1H NMR calculations is necessary especially for acidic protons in order to obtain accurate values. The equilibrium geometries, harmonic frequencies, and FT-IR intensities of the metal complexes were determined and analyzed at DFT level of theory utilizing LANL2DZ basis sets. NBO analysis revealed that the strong coordination bonds result from donation of electron density from a lone pair orbital on the nitrogen atoms to the acceptor metal molecular orbitals e.g. (LP(1)N11 → σ*(Pt-Cl22)) and (LP(1)N21 → σ*(Pt-Cl23)). The studied compounds have the capacity of inhibiting the metabolic growth of the investigated bacteria to different extents. In addition, the complexes are toxic against three cell lines of different origin and represent an interesting class of new compounds from the viewpoint of their physicochemical and structural properties. The IC_{50} (μg/ml) values were always twice those of the cis-platin. Based on the results of elemental analysis, spectral, thermal and conductance values, square planar geometry is suggested for the complexes with the general formula; $[MCl_2]$ (M = Pd and Pt) and $[PdL(OH_2)_2]\bullet 2X\bullet zH_2O$ (X = Br, I, z = 2; X = SCN, z = 1; X = NO_3, z = 0).

Acknowledgments

We would like to extend our grateful thanks to Dr. Mohamed Elshakre, assistant professor of physical chemistry, Chemistry Department, Faculty of Science, Cairo University for allowing us to use his version of the *GAUSSIAN03* package of programs. Deep thanks to Prof. Dr. Samia Showman, professor of medical

biochemistry, National Cancer Centre, Cairo University, for the great helps and support during the biological part.

Appendix. Supplementary material

CCDC 762681 contains the supplementary crystallographic data for this paper. These data can be obtained free of charge via www.ccdc.cam.ac.uk/conts/retrieving.html (or from the Cambridge Crystallographic Data Centre, 12, Union Road, Cambridge CB2 1EZ, UK; fax: +44 1223 336033).

Appendix. Supplementary data

Supplementary data associated with this article can be found, in the online version, at doi:10.1016/j.ejmech.2011.11.008.

References

[1] (a) I.H. Krakoff, in: M. Nicali (Ed.), Platinum and Other Metal Coordination Compounds in Cancer Chemotherapy": Clinical Application of Platinum Complexes, Martinus Nijhoff, Boston, MA, 1988, p. 351;
(b) E.R. Jamieson, S.J. Lippard, Chem. Rev. 99 (1999) 2467–2498.
[2] I. Kostova, Recent Patents Anti-Cancer Drug Discov. 1 (2006) 1–22.
[3] (a) S. Roy, J.A. Westmaas, F. Buda, J. Reedijk, J. Inorg. Biochem. 103 (2009) 1278–1287;
(b) D. Montagner, V. Gandin, C. Marzano, B. Longato, J. Inorg. Biochem. 105 (2011) 919–926.
[4] (a) K. Akdi, R.A. Vilaplana, S. Kamah, J.A.R. Navarro, J.M. Salas, F. González-Vílcheza, J. Inorg. Biochem. 90 (2002) 51;
(b) A. Matilla, J.M. Tercero, N.H. Dung, B. Voissat, J.M. Pérez, C. Alonso, D. Martín-Ramos, J. Niclós-Gutiérrez, J. Inorg. Biochem. 55 (1994) 235.
[5] (a) F. Gumus, G. Eren, L. Acik, A. Celebi, F. Ozturk, R. Ilikci Sagkan, S. Gur, A. Ozkul, A. Elmali, Y. Elerman, J. Med. Chem. 52 (5) (2009) 1345–1357;
(b) M. Goekce, S. Utku, S. Guer, A. Oezkul, F. Gumus, Eur. J. Med. Chem. 40 (2) (2005) 135–141;
(c) F. Gumus, O. Algul, G. Eren, H. Eroglu, N. Diril, S. Gur, A. Ozkul, Eur. J. Med. Chem. 38 (5) (2003) 473–480;
(d) F. Gumus, A.B. Demirci, T. Oezden, H. Eroglu, N. Diril, Pharmazie 58 (5) (2003) 303–307;
(e) F. Gumus, I. Pamuk, T. Oezden, S. Yildiz, N. Diril, E. Oksuzoglu, S. Gur, A. Ozkul, J. Inorg. Biochem. 94 (3) (2003) 255–262.
[6] (a) V. Rajendiran, M. Murali, E. Suresh, S. Sinha, K. Somasundaram, M. Palaniandavar, Dalton Trans. (2008) 148;
(b) J. Mann, A. Baron, Y. Opoku-Boahen, E. Johansson, G. Parkinson, L.R. Kelland, S. Neidle, J. Med. Chem. 44 (2001) 138;
(c) P.K. Naithani, V.K. Srivastava, A.K. Saxena, J.P. Barthwal, T.K. Gupta, K. Shanker, Indian J. Exp. Biol. 28 (1990) 1145;
(d) N.M. Goudgaon, V. Dhondiba, A. Vijayalaxmi, Indian J. Heterocycl. Chem. 13 (2004) 271.
[7] (a) E. Bouwmann, W.L. Driessen, J. Reedijk, Coord. Chem. Rev. 104 (1990) 143;
(b) M.A. Puja, T.D. Bharamgouda, N.D. Sathyanarayna, Trans. Met. Chem. 13 (1988) 423.
[8] (a) Phillips, J. Chem. Soc. (1928) 2393;
(b) H. Skolnik, J. Miller, A.R. Day, J. Am. Chem. Soc. 65 (1943) 1854.
[9] A. Skoog, D.M. West, Fundamentals of Analytical Chemistry. Thomson, Brooks, Cole, New York, 2004.
[10] A.L. Spek, J. Appl. Cryst. 36 (2003) 7.
[11] A.L. Spek, Program for Reduction of CAD-4 Data. University of Utrecht, The Netherlands, 1996.
[12] A. Altomare, G. Cascarano, C. Giacovazzo, A. Guagliardi, M.C. Burla, G. Polidori, M. Camalli, J. Appl. Cryst. 27 (1994) 435.
[13] S. Mackay, C.J. Gilmore, C. Edwards, N. Stewart, K. Shankland, Maxus Computer Program for the Solution and Refinement of Crystal Structures (1999) Bruker Nonius, The Netherlands, MacScience, Japan & The University of Glasgow.
[14] C.K. Johnson, ORTEP–II. A Fortran Thermal–Ellipsoid Plot Program Report ORNL-5138. Oak Ridge Natlonal Laboratory, Oak Ridge, Tennessee, USA, 1976.
[15] (a) A.D. Becke, J. Chem. Phys. 98 (1993) 5648;
(b) C. Lee, W. Yang, R.G. Parr, Phys. Rev. B. 37 (1998) 785.
[16] M.J. Frisch, G.W. Trucks, H.B. Schlegel, G.E. Scuseria, M.A. Robb, J.R. Cheeseman, V.G. Zakrzewski, J.A. Montgomery, R.E. Stratmann, J.C. Burant, S. Dapprich, J.M. Millam, A.D. Daniels, K.N. Kudin, M.C. Strain, O. Farkas, J. Tomasi, V. Barone, M. Cossi, R. Cammi, B. Mennucci, C. Pomelli, C. Adamo, S. Clifford, J. Ochterski, G.A. Petersson, P.Y. Ayala, Q. Cui, K. Morokuma, D.K. Malick, A.D. Rabuck, K. Raghavachari, J.B. Foresman, J. Cioslowski, J.V. Ortiz, A.G. Baboul, B.B. Stefanov, G. Liu, A. Liashenko, P. Piskorz, I. Komaromi, R. Gomperts, R.L. Martin, D.J. Fox, T. Keith, M.A. Al-Laham, C.Y. Peng, A. Nanayakkara, C. Gonzalez, M. Challacombe, P.M.W. Gill, B.G. Johnson, W. Chen, M.W. Wong, J.L. Andres, M. Head-Gordon, E.S. Replogle, J.A. Pople, GAUSSIAN 03 (Revision A.9). Gaussian, Inc., Pittsburgh, 2003.
[17] A. Frisch, A.B. Nielson, A.J. Holder, GAUSSVIEW User Manual. Gaussian Inc, Pittsburgh, PA, 2000.
[18] R. Ditchfield, Chem. Phys. 76 (1972) 5688.
[19] D.P. Singh, K. Kumar, C. Sharma, Eur. J. Med. Chem. 44 (2009) 3299–3304.
[20] National Committee for Clinical Laboratory Standards, NCCLS Approval Standard Document M2-A7. Vilanova, PA, 2000.
[21] P. Skehan, R. Storeng, J. Natl. Cancer Inst. 42 (1990) 1107–1112.
[22] C.M. Lozano, O. Cox, M.M. Muir, J.D. Morales, J.L. Rodríguez-Cabáin, P.E. Vivas-Mejfa, F.A. Gonzalez, Inorg. Chim. Acta 271 (1998) 137–144.
[23] (a) G. Rauhut, P. Pulay, J. Phys. Chem. 99 (1995) 3093–3100;
(b) J.A. Pople, H.B. Schlegel, R. Krishnan, J.S. Defrees, J.S. Binkley, M.J. Frisch, R.A. Whiteside, Int. J. Quantum Chem.: Quantum Chem. Symp 15 (1981) 269.
[24] (a) M.W. Ellzy, J.O. Jensen, H.F. Hameka, J.G. Kay, D. Zeroka, Spectrochim. Acta 57A (2001) 2417;
(b) J.O. Jensen, A. Banerjee, C.N. Merrow, D. Zeroka, J.M. Lochner, J. Mol. Struct. Theochem. 531 (2000) 323;
(c) J.O. Jensen, D. Zeroka, J. Mol. Struct. Theochem. 487 (1999) 267.
[25] O. Sala, N.S. Goncalves, L.K. Noda, J. Mol. Struct. 411 (2001) 565–566.
[26] (a) J.R. Ferraro, Low Frequency Vibrations of Inorganic and Coordination Compounds. Plenum Press, N. Y., 1971;
(b) R.J.H. Clark, C.S. Williams, Inorg. Chem. 4 (1965) 350.
[27] K. Nakamoto, Infrared and Raman Spectra of Inorganic and Coordination Compounds', Part B: Applications in Coordination, Organometallic, and Bioinorganic Chemistry, sixth ed.. John Wiley & Sons Inc., New Jersey, 2009.
[28] W. Nawrocka, B. Sztuba, M.W. Kowalaka, H. Liszkiewicz, Farmaco 59 (2004) 83.
[29] (a) E. Bednarek, J.C. Dobrowolski, K. Dobrosz-Teperek, L. Kozerski, W. Lewandowski, A.P. Mazurek, J. Mol. Struct. 554 (2000) 233–243;
(b) F.S. Miranda, F.G. Menezes, J. Vicente, A.J. Bortoluzzi, C.Z. Ademir- Neves, N.S. Gonçalves, J. Mol. Struct. 938 (2009) 1–9.
[30] R.M. Issa, A.A. Hassanein, I.M. El-Mehasseb, R.I. Abed. El-Wadoud, Spectrochim. Acta Part A 65 (2006) 206–214.
[31] (a) M. Krishnamurthy, P. Phaniraj, S.K. Dogra, J. Chem. Soc. Perkin Trans. (1986) 1917–1925 (and the references therein);
(b) A.K. Mishra, S.K. Dogra, Bull. Chem. Soc. Jpn. 58 (1985) 3587;
J. Photochem. 31 (1985) 333;
Indian J. Phys., Sect. B 54 (1984) 480;
Spectrochim. Acta. Part A 39 (1983) 609.
[32] R.M. Issa, S.A. El-Daly, N.A. El-Wakiel, Spectrochim. Acta Part A 59 (2003) 723–728.
[33] C.K. Jorgensen, Absorption Spectra and Chemical Bonding in Complexes. Pergamon Press, London, 1964.
[34] (a) A.B.P. Lever, Inorganic Electronic Spectroscopy, second ed. Elsevier, Amsterdam, 1982, pp. 544–552;
(b) S.P. Perlepes, P. Jacobs, H.O. Desseyn, J.M. Tasangaris, Spectrochim. Acta 43A (1987) 771.
[35] (a) I. Lakomska, M. Barwiolek, E. Szlyk, Tran. Met. Chem. 32 (2007) 70;
(b) A. Bakalova, H. Varbanov, R. Buyukliev, G. Momekov, D. Ivanov, J. Therm. Anal. Calorimetry 95 (2009) 241–246.
[36] D.R. Lide, Handbook of Chemistry and Physics, second ed. CRC, 2008.
[37] A.W. Coats, J.P. Redfern, Nature 201 (1964) 68.
[38] H.H. Horowitz, G. Metzger, Anal. Chem. 85 (1963) 1464.
[39] B.D. Cullity, Elements of X-ray Diffraction, second ed.. Addison-Wesley Inc., 1993.
[40] N. Vijayan, R. Ramesh Babu, R. Gopalakrishnan, P. Ramasamy, W.T.A. Harrison, J. Crystal Growth 262 (2004) 490–498.
[41] D.N. Neogi, P. Das, A.N. Biswas, P. Bandyopadhyay, Polyhedron 25 (2006) 2149.
[42] (a) R.W. Hay, T. Clifford, P. Lightfoot, Polyhedron 17 (20) (1998) 3575–3581;
(b) X. Jing-Yuan, G. Wen, L. Ling, Y. Shi-Ping, C. Peng, L. Dai-Zheng, J. Zong-Hui, J. Mol. Struct. 644 (2003) 23–27.
[43] R. Wysokiński, D. Michalska, J. Comput. Chem. 22 (9) (2001) 901–912.
[44] A.E. Reed, L.A. Curtiuss, F. Weinhold, Chem. Rev. 88 (1988) 899.
[45] I. Fleming, Frontier Orbitals and Organic Chemical Reactions. Wiley, London, 1976.
[46] W.T. Shier, Mammalian Cell Culture on $5 a Day: A Lab Manual of Low Cost Methods. University of the Philippines, Los Banos, 1991, pp 64.
[47] M. Pérez-Cabré, G. Cervantes, V. Moreno, M.J. Prieto, J.M. Pérez, M. Font-Bardia, X. Solans, J. Lnorg. Biochem. 98 (2004) 510–521.